ACS Photonics

pubs.acs.org/journal/apchd5

Article

Deep Generative Modeling and Inverse Design of Manufacturable Free-Form Dielectric Metasurfaces

Ibrahim Tanriover, Doksoo Lee, Wei Chen,* and Koray Aydin*

Cite This: *ACS Photonics* 2023, 10, 875−883

Read Online

ACCESS | Metrics & More | Article Recommendations | Supporting Information

ABSTRACT: Conventional approaches on design and modeling of metasurfaces employ accurate simulation methods. However, these methods require considerable computational power and time for every simulation, making them computationally expensive in the long run. To address this high computational cost and learn compact yet expressive design representations of high-dimensional meta-atoms for efficient design optimization, deep learning (DL) based approaches have emerged as an alternative solution and numerous applications have been demonstrated in recent years. However, there are still outstanding challenges in DL-assisted modeling and design that need to be overcome, such as limited degrees of design freedom, insufficient generalizability of models, and poor fabrication feasibility of final designs. Here, concurrently addressing these challenges, we propose an end-to-end framework for generative modeling and inverse design of dielectric free-form metasurfaces. The framework is generic, as it can accommodate a variety of physical scenarios including dispersion, incident polarization, and operation wavelength using a single data set and model. We develop a shape generation method to generate an inclusive, free-form, and feasible meta-atom library with manufacturability considerations. A forward model that exhibits improved generalizability in terms of material dispersion, polarization, and spectral window of operation is constructed using neural networks. In the final stage, an inverse design of free-form yet manufacturable metasurfaces is realized. As a proof-of-concept, forward design of a meta-lens and inverse optimization of a polarization filter and a quarter-wave plate are demonstrated.

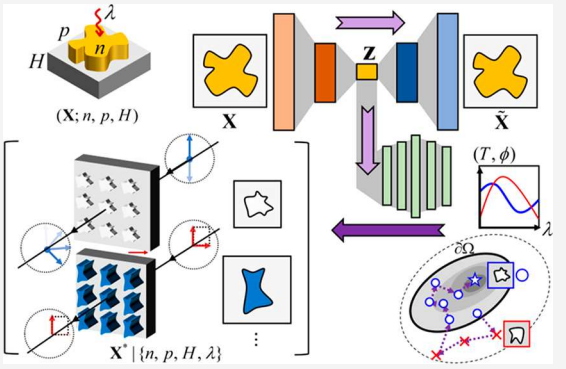

KEYWORDS: *deep learning, manufacturability, all-dielectric, inverse design, polarization, dispersion*

Conventional metasurface simulation, design tools, and approaches rely on full electromagnetic simulations to calculate the optical response of nanophotonic structures. These simulation methodologies are based on either finite elements (FEM) or finite difference time domain (FDTD) methods and provide accurate and deterministic predictions.[1−11] However, the high computational cost of current methods becomes a limiting factor, especially with increased structural complexity.

Deep learning (DL) approaches have emerged as an alternative tool to address the high computational cost of conventional simulation tools as well as to learn compact design reparameterization of intricate metasurface geometries.[12−35] DL has been used for forward modeling of metasurfaces to obtain instant and highly accurate predictions of optical response from a given structure. Numerous examples of forward modeling, including models of multilayered structures,[29,30] predefined meta-atoms,[11,17,18] and arbitrary polygons,[31,32] have been realized. The inverse problem, designing the corresponding structure from a given optical response, is also studied extensively. Three main approaches of DL, which are supervised learning,[17,33] unsupervised learning,[22,25−27] and reinforcement learning,[34] have been applied to the inverse problem for various metasurface applications.[35]

However, from both perspectives of forward problem and inverse design, DL-assisted modeling and design have several challenges to address. One of these problems is limited degrees of design freedom. Most of the pioneering works resort to well-known fundamental building blocks as "meta-atom baselines".[17−21] Many of these only consider parametric variations of these baseline structures, such as radius of cylindrical meta-atoms or thickness of alternating layers, which significantly limit the design freedom *a priori*.[17−21] To explore beyond the baseline structures, deep generative model-based approaches have been reported, yet the resulting geometries are still limited to perturbations of the predefined building blocks.[22] Although some recent studies model quasi-free-form structures,[23,24] they still have limited degrees of freedom due to

Special Issue: Optimized Photonics and Inverse Design

Received: June 29, 2022
Published: September 22, 2022

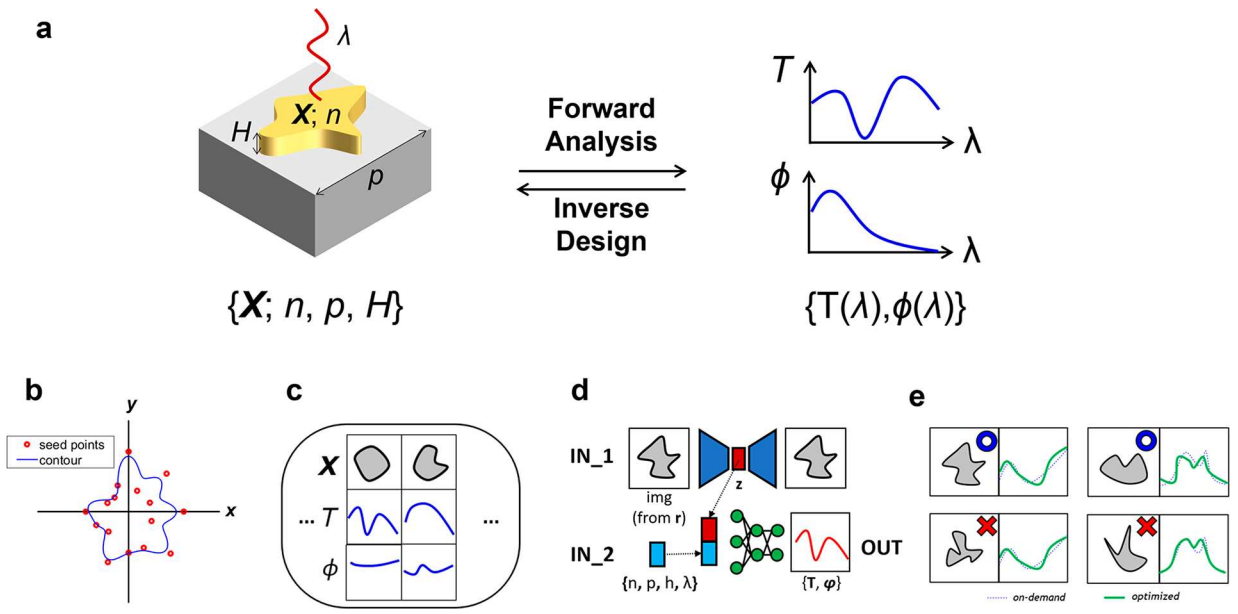

Figure 1. (a) A schematic of forward modeling and inverse design. The design variables encompass planar shape, refractive index, periodicity, and height. Given a set of design variables, forward analysis yields the frequency response of transmission and phase delay. Reversely, inverse design identifies shape given on-demand spectra. (b–e) Overview of the proposed procedure. (b) Random shape generation based on curvature constraint. (c) Database generation by wave simulation. (d) Forward net as a composite of an autoencoder and fully connected layers. (e) Inverse optimization given the on-demand spectra under fabrication constraints.

both the low resolution of pixelated unit cells and limited shape variations of their building blocks.

DL-assisted metasurface design also suffers from limited model generalizability. Even with substantial training data (typically $\sim O(10^4)$) fed into DL models, their applicability is confined by the training data;[18−24] for instance, if the data set only includes meta-atoms excited by an *x*-polarized incidence, the DL model trained on this data set does not generalize to the cross-polarized illumination. Accommodating any changes in the problem setting, such as polarization of illumination, operating spectral range, or material properties, requires training of either a new model from scratch or an updated one with a new data set, which results in a repetition of the computationally expensive data generation and training processes.

Additionally, it is not straightforward for DL-based approaches to impose fabrication constraints in inverse design. Among many relevant works, conditional generative models have gained special attention primarily due to the ease of using them for "on-the-fly" inverse design, which circumvents arduous iterative geometric optimization in high-dimensional space.[22,25,26] However, inverse design under fabrication constraints has not been reliably addressed for DL-assisted design. Existing works (i) resort to morphological postprocessing without considering the performance deviation at the system level,[22,25] (ii) do not take fabrication limitations into account at all, or (iii) impose them only in low-dimensional design space such as one-dimensional meta-grating.[28]

In this paper, we propose and demonstrate an inclusive framework for deep generative modeling and inverse design of manufacturable free-form metasurfaces considering the limitations of lithography-based top-down fabrication processes. Our framework concurrently addresses the aforementioned issues summarized as (i) limited design freedom, (ii) insufficient model generalizability, and (iii) poor fabrication feasibility. The framework is comprehensive as it can accommodate a variety of operating conditions and meta-atom structures while ensuring fabrication feasibility. Figure 1 provides an overview of the framework. First, to increase the design freedom and ensure fabrication feasibility in the training data set, we wish to generate a library of manufacturable free-form meta-atoms. To this end, we propose a new shape generation method considering fabrication constraints and create a diverse shape library. Second, to address insufficient model generalizability, a forward network that maps meta-atom to optical response is constructed, where the unit cell is specified by periodicity, cross-section (shape), height, and refractive index of the meta-atom. Our forward model exceeds the boundaries of the training data set; the model generalizes the solution to different spectral range of operations, material dispersions, and incident polarizations. Lastly, to address fabrication feasibility, fabrication-constrained inverse optimization in the latent space of the forward net follows to produce metadevices under the limitations of lithography-based top-down fabrication processes. The optimization involves multiple constraints including local curvature, minimum feature size, and optical responses. To search optimal meta-atoms under the constraints without case-specific parameter tuning, a genetic algorithm based on feasibility-first ranking is employed.[36] We demonstrate the efficacy of the proposed framework via two metadevice design cases, namely broadband polarization filter and quarter-wave plate.

RESULTS AND DISCUSSION

As a data-driven method, DL's performance significantly depends on the data set. Thus, creating an inclusive forward model requires a data set that is unbiased and comprehensive in terms of the design space. Here, the design space consists of the 2D cross-section (or the shape), periodicity (p), height (H), and refractive index (n) of the unit structure (or the meta-atom). For the first three design variables, 50 sets of values are chosen by Latin hypercube sampling[37] within

https://doi.org/10.1021/acsphotonics.2c01006
ACS Photonics 2023, 10, 875−883

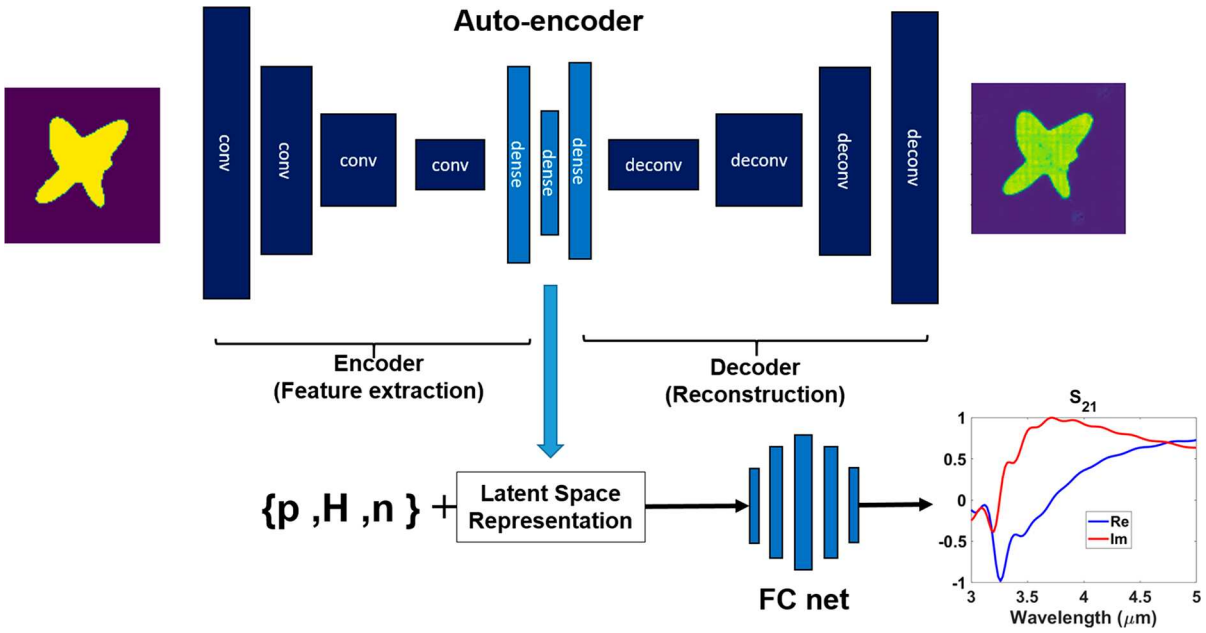

Figure 2. Schematic of the FWD net. The network consists of an autoencoder and a fully connected DNN (FC net). The autoencoder consist of 4 convolution, 5 hidden, and 4 deconvolution layers in the given order. The cross-section of the meta-atom is represented as a 100 × 100 pixel image. The hidden features are extracted from the image and compressed into 16 parameter latent vectors by the encoder. The original image is reconstructed from the latent vector by the decoder. FC net has 5 fully connected hidden layers with 40, 120, 240, 120, and 40 neurons, respectively. The input of the FC includes refractive index (n), wavelength-normalized geometric parameters of unit cell (p/λ, H/λ), and the latent space representation of the meta-atom cross-section. The final output is a complex-valued transmission (S_{21}) coefficient.

predefined ranges. To create a comprehensive data set, the cross sections should be arbitrary, unbiased, and free-form. Additionally, we require our meta-atoms constituting the data set to be manufacturable.

In this work, manufacturability is defined by the constraints imposed by the lithography-based top-down fabrication processes such as minimum feature size and minimum radius of curvature. We also impose a maximum size limit to ensure uncoupled operation between adjacent unit cells. To generate arbitrary, free-form, yet fabricable meta-atoms, we propose a shape generation method, in which a predefined set of seed points are randomly distributed over the xy plane. Then, these points are connected by a smooth, closed curve generated using constrained nonlinear regression (see Figure 1b and SI-1). This method provides analytical expressions for the contour of the shapes and enables direct control of size and curvature. Meanwhile, the constrained fitting involves nonuniform deviations of the seed points. To reduce the sampling redundancy induced by the constrained design space, determinantal point processes[38] that favor a set of repulsive items are employed as a subset sampler. As a result, a total number of 20,000 samples combining 400 shapes and 50 parameter sets are generated. The sample-label (unit cell-optical response) pairs are created using full-wave electromagnetic simulations. A detailed discussion on the data generation process is provided in the Supporting Information.

We apply wavelength normalization[17] to achieve spectral generalizability beyond the training data set and to remove the dimensional mismatch between metasurface design space and the optical response.[17,18] The height and the periodicity are directly normalized to the wavelength vector. On the other hand, the meta-atom shapes are represented as images with a 100 × 100 pixel resolution. To apply wavelength normalization to these shapes, the cross-sectional contour is scaled with the operation wavelength. We fixed the image frame with the dimensions of the largest normalized periodicity in order to keep both the pixel number and size constant during scaling. However, as the wavelength normalization involves the multiplication of the number of samples with the number of frequency points, which is 101 frequency points that create >4,000,000 instances in our case, a large time and memory requirement arise.

To overcome this limitation, the problem is divided into two parts: (1) the image representing the cross-section of the meta-atom and (2) structural parameters including the height of meta-atom, the periodicity of the unit cell, and the refractive index of the material. Two independent networks are constructed to solve each component of the problem, an autoencoder and a fully connected NN (FC net) as seen in Figure 2.

The autoencoder extracts important features from the cross-section images (Figure 2). It compresses 2D image representation into a latent vector representation from which the original cross-section can be reconstructed with an acceptable loss of geometrical details. Harnessing the on-the-fly forward analysis of meta-atoms, we apply data augmentation without any additional cost by rotating the shapes 8 times by 45°. To apply the wavelength normalization, the images are scaled with 10 frequency points that are randomly selected. Total instances used in training data of the autoencoder become 32,000, consequently removing the large time and memory requirement. Concatenating the resulted latent vector with the numeric parameters (*i.e.*, n, p, H), we construct the input vector of the FC net as seen in the Figure 2. The FC net maps this input vector to the optical response (*i.e.*, transmission and phase delay). The combination of these networks (autoencoder and FC net) creates the forward network (FWD net), for predicting the optical response of a metasurface unit

https://doi.org/10.1021/acsphotonics.2c01006
ACS Photonics 2023, 10, 875−883

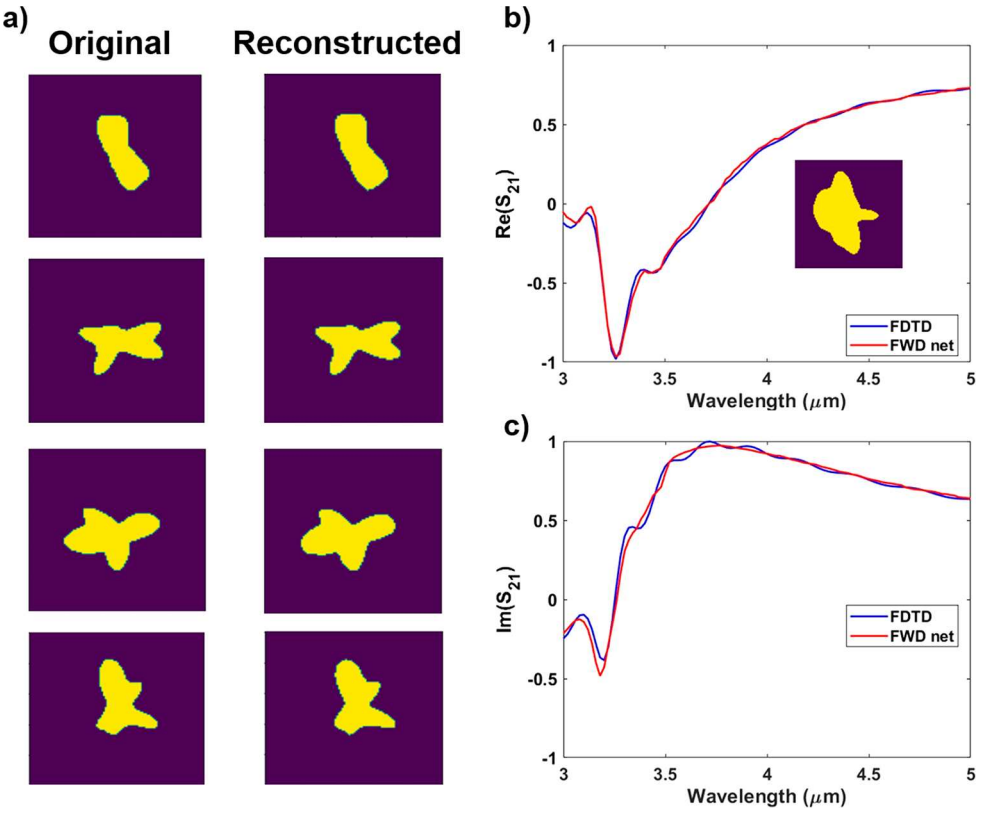

Figure 3. (a) Comparison of original and reconstructed images. (b,c) Comparison of simulated and predicted transmission coefficients of exemplary samples from the validation set (blue line: simulation and red line: prediction). The prediction MSE of this sample is 9.0×10^{-4}. The cross-section of the example meta-atom is shown in the inset of (b).

cell given the cross-section, height, periodicity, and refractive index.

For the training and the test of both the autoencoder and FC net, the means squared error (MSE) loss is used as the model performance metric. The overall training/test MSEs are $2.0 \times 10^{-3}/4.2 \times 10^{-3}$ and $1.0 \times 10^{-3}/2.0 \times 10^{-3}$ for the autoencoder and FC net, respectively. Together with error distributions and learning curves that are provided in the Supporting Information, the low and consistent training/test error values indicate that successful learning is achieved without overfitting.

To demonstrate overall performance of the FWD net, we compare original-reconstructed images and the predicted (simulated) optical response of a sample from the unseen validation set in Figure 3 (see the Supporting Information for additional examples). There is a good agreement between the original images and the reconstructed ones as seen in Figure 3a. Meanwhile, Figure 3b,c indicates sound predictive performance over optical responses. As a proof-of-concept for metadevice design, forward design of a metalens is demonstrated in Supporting Information.

The network architecture and wavelength normalization approach[17] provide extended generalization capabilities to the FWD net beyond the feature and operation space defined by the data set. One of these unique properties is spectral generalizability, which is the ability to generalize the solution within one spectral range to other spectral ranges. Spectral generalizability depends on the wavelength scalability of electromagnetic problems and is inherited from the wavelength normalization process[17] (see Supporting Information for detailed explanations). To demonstrate the spectral generalizability capability of the FWD net, we generated a set of samples in the visible range (400 to 700 nm), which corresponds to 7.5 times larger frequencies than the data set's frequency range. As seen from the example sample shown in Figure 4a,b, the FWD net maintains its success in a spectral range that is not covered by the training data [see the Supporting Information for more examples in visible and also near-infrared (1.5 to 2.5 μm) ranges].

Another generalization capability of our FWD net is modeling dispersive materials without explicit training. As an outcome of wavelength normalization, our network makes predictions for each frequency point independently. The refractive index differences between different frequencies do not affect each other. As a result, the optical response is accurately predicted regardless of the dispersion. As an example, we define a lossless dielectric with a highly dispersive refractive index as seen in the inset of Figure 4c. Despite being trained for nondispersive dielectrics only, the FWD net accurately predicted the optical response of a dispersive meta-atom, as seen in Figure 4c,d.

Additionally, the FWD net can predict optical responses for different incident polarizations although all samples in our library are generated considering only the x-polarized incidence. Due to the symmetry of the problem, the optical response of a structure under y-polarized incidence will be the same as the optical response of the 90° rotated version of the structure under x-polarization. As we introduce shape rotations by the data augmentation step applied before the training, our autoencoder can distinguish, reconstruct, and compress the rotated cross sections. As a result, the FWD net maintains high prediction accuracy for the rotated meta-atoms. As a

https://doi.org/10.1021/acsphotonics.2c01006
ACS Photonics 2023, 10, 875−883

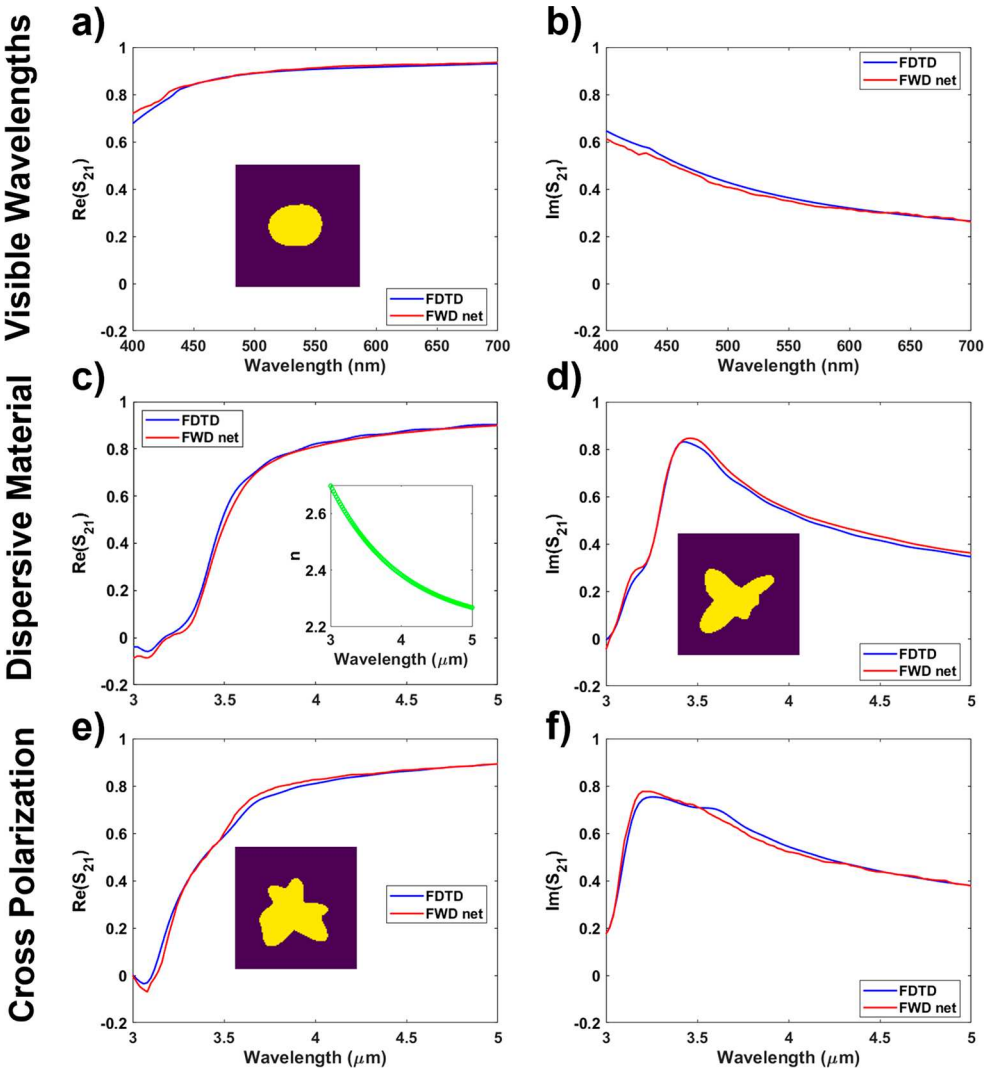

Figure 4. Comparison of predicted and simulated transmission response of (a,b), an example in the visible wavelengths (400−700 nm), (c,d) an example of a dispersive material, and (e,f) an example under *y*-polarized illumination. The prediction MSEs are (a,b) 2.1×10^{-4}, (c,d) 3.5×10^{-4}, and (e,f) 3.8×10^{-4}. The parameters are as follows: (a,b) p = 300 nm, H = 300 nm, and n = 2.15, (c,d) p = 2.38 μm, H = 2.0 μm, and n is shown in the inset, and (e,f) p = 2.48 μm, H = 1.96 μm, and n = 2.31. The cross sections of the example meta-atoms are shown in the figure insets.

demonstration, several samples are selected from the unseen validation set and simulated with *y*-polarized incidence. As seen in Figure 4e,f, the FWD net can predict the optical response of meta-atoms under *y*-polarized illumination as well. This result indicates that our model is unlimited with polarization of incidence as any polarization can be expressed as superposition of two orthogonal states (x and y, in this case).

INVERSE OPTIMIZATION

The purpose of inverse design in this work is to identify a manufacturable meta-atom shape given target functionalities of a metadevice. A symbolic formulation of the inverse problem reads:

$$\underset{\boldsymbol{X}}{\operatorname{argmin}}\, J(T(\boldsymbol{X}, \lambda|n, p, H), \phi(\boldsymbol{X}, \lambda|n, p, H)) \tag{1}$$

$$\text{subject to } \kappa \leq \kappa_{\max} \tag{2}$$

$$r \leq r_{\max} \tag{3}$$

$$r = F(\boldsymbol{\varphi})^* \boldsymbol{w},\ r'(\boldsymbol{\varphi}) = F'(\boldsymbol{\varphi})^* \boldsymbol{w},\ r''(\boldsymbol{\varphi}) = F''(\boldsymbol{\varphi})^* \boldsymbol{w} \tag{4}$$

where J is a performance metric expressed as a function of either transmission T or phase ϕ; $\boldsymbol{X}$ is a planar shape of a meta-atom; κ is local curvature of a meta-atom; and $\kappa_{\max}$ is the allowable maximum curvature set as $\kappa_{\max}$ = 0.025 nm^{-1}. The performance metric J takes the planar shape $\boldsymbol{X}$ as an implicit argument. Eq 3 is imposed $r \leq r_{\max}$ = 850 nm as a constraint on the feature size of a meta-atom for uncoupled operation. The secondary design variables $\{n, p, H\}$ remain unchanged during each optimization run. We use n = 3.5, p = 2 μm, and H = 2 μm, unless otherwise stated.

We employ genetic algorithms (GAs) for inverse design. Our baseline formulation is categorized as a single-objective optimization problem under multiple constraints (curvature, feature size, etc.). Hence, efficient constraint handling is of top importance for the inverse design. GAs can bypass case-specific tuning of constraint parameters through feasibility-first population ranking.[36] By avoiding the manual tuning of constraint parameters for individual design cases, a variety of unit cell optimization problems can be addressed. In addition,

https://doi.org/10.1021/acsphotonics.2c01006
ACS Photonics 2023, 10, 875−883

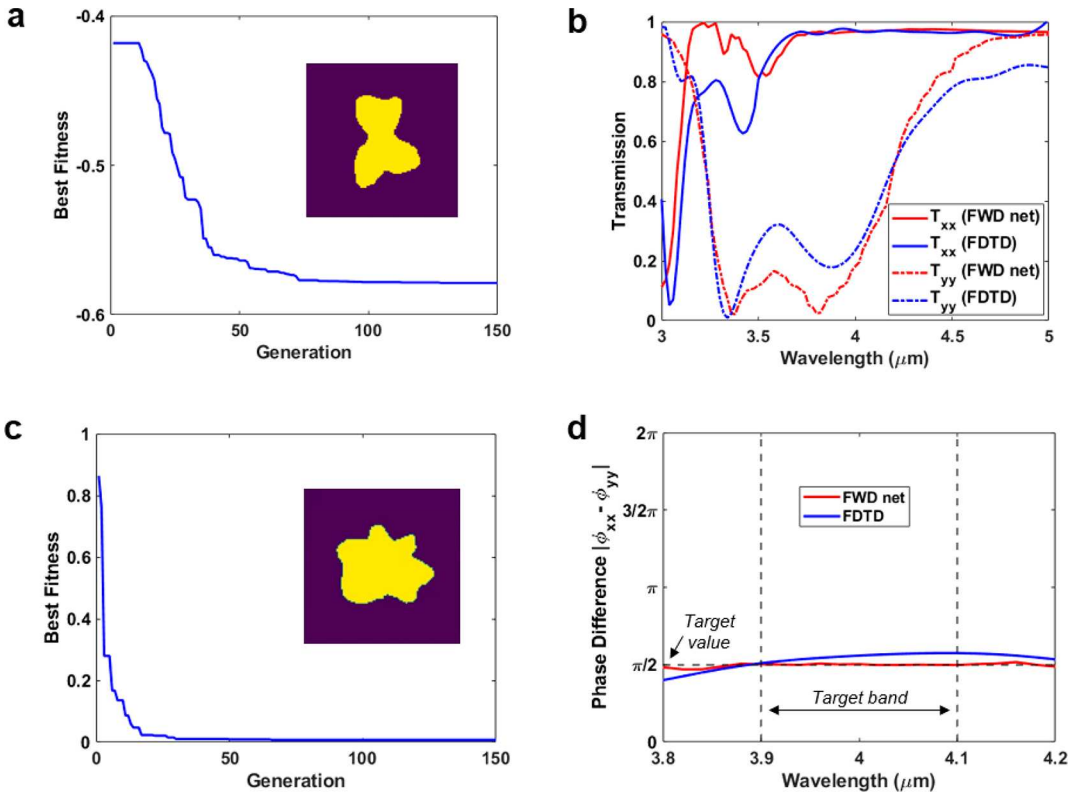

Figure 5. Inverse optimization results. (a,b) Polarization filter design. (a) Optimization history of the best fitness of J_1 and optimized shape. (b) Transmission spectra. (c,d) Quarter-wave plate design. (c) Optimization history of the best fitness of J_2 and optimized shape. (d) Differences between the two phase shift components where the target is $\pi/2$.

the population-based, derivative-free evolutionary search mitigates the issues of both local optimality and initial dependence that gradient-based design search mostly suffers from. With the aid of the FWD net, it is tractable to perform an exhaustive search of GA in the compact latent space that captures major design variations and fabrication feasibility.

As a proof-of-concept for metadevice applications, the proposed inverse optimization result of a polarization filter is presented. The desired functionality is to provide selective transmission between two orthogonal polarization states. The major responses of interest are two transmission components (T_{xx} and T_{yy}). An asscoiated figure-of-merit can be quantified as the difference between the two components. Built on the generic formulation in eqs 1−4), we formulate the optimization problem as

$$\underset{\mathbf{z}}{\operatorname{argmin}} J_1 = -\sum_j |T_{xx}(\mathbf{z}, \lambda_j|n, p, H) - T_{yy}(\mathbf{z}, \lambda_j|n, p, H)| \tag{5}$$

$$\text{subject to } \kappa(x, y) = \frac{|x''y' - x'y''|}{((x')^2 + (y')^2)^{3/2}} \le \kappa_{\max} \tag{6}$$

with eqs 3 and 4, where J_1 is the figure-of-merit of polarization filters defined as the absolute difference between the two transmission components; $\boldsymbol{z}$ is the latent vector of FWD net that represents the structure of the meta-atom; and eq 6 is the local curvature constraint defined in the Cartesian coordinate system. Assuming T_{xx} is the transmission of an arbitrary shape, T_{yy} is quickly computed by rotating a meta-atom shape by 90° and passing it to the FWD net. No target band is specified *a priori*. Figure 5a displays the GA result after 150 generations where the size of the population is 80. The decreasing trend of the best fitness shows significant performance improvements. The optical responses of the smooth final design show high-contrast transmission between the two components over a wide range of band (Figure 5b).

Adding another metadevice application, we also performed the proposed inverse optimization for a quarter-wave plate (Figure 5c,d). The device transforms linear polarization to circular polarization, and vice versa. The target functionality demands $\pi/2$-phase difference between the two orthogonal phase components $\boldsymbol{\phi}_{xx}$ and $\boldsymbol{\phi}_{yy}$. In addition, high transmission is required for each direction, which can be interpreted as two additional constraints for inverse optimization. We formulate the quarter-wave design problem as

$$\underset{\mathbf{z}}{\operatorname{argmin}} J_2 = \sum_j ||\phi_{xx}(\mathbf{z}, \lambda_j|n, p, H) - \phi_{yy}(\mathbf{z}, \lambda_j|n, p, H)| - \pi/2| \tag{7}$$

$$\text{subject to } T_{xx}(\mathbf{z}, \lambda_j|n, p, H),\ T_{yy}(\mathbf{z}, \lambda_j|n, p, H) \ge T_{thre} \tag{8}$$

with eqs 3, 4, and 6, where J_2 is the performance metric used for the inverse design of quarter-wave plates. T_{thre} is the threshold value that reflects the high-transmission requirements, which is set as 0.75. Figure 5d shows the optimization result given a target band of 3.9−4.1 μm. The optimization history of the figure-of-merit J_2 in Figure 5c shows a sharp decrease at the early stage, followed by a long plateau stage. The free-form final design meets the high transmission requirement as well as the two fabrication constraints.

To validate the inclusiveness of the proposed framework over broad design cases, we tested another optimization run for

https://doi.org/10.1021/acsphotonics.2c01006
ACS Photonics 2023, 10, 875−883

a polarization filter with setting the secondary design variables as {n = 4.0 (Ge), p = 2.3 μm, H = 1.7 μm}. The result yields an optimized meta-atom shape of which performance is slightly better than the case where {n = 3.5, p = 2.0 μm, H = 2.0 μm}, mainly due to the higher refractive index, with a completely different trend of transmissions (Figure S9). The result corroborates the comprehensive nature of our framework: it simultaneously covers free-form shape variations, the secondary design variables, and the fabrication constraints, by the single model and single database. Under large variations of off-design conditions, both continuum-based topology optimization[36,39] or automatic differentiation[40] must run from scratch for every condition, with manual handling of constraints taken into account. Conditional generative networks[22,25,26] have potential to cover a broad range of design cases, yet existing works are dedicated to design under a fixed set of secondary design variables and not able to handle design constraints reliably.

CONCLUSION

In this work, for deep generative modeling and inverse design of manufacturable free-form metasurfaces, we presented a comprehensive framework that simultaneously addresses three core challenges of DL based photonic metasurface design: limited design freedom, insufficient model generalizability, and poor fabrication feasibility. At the first step, we constructed a shape generation method that creates arbitrary free-form geometries while imposing manufacturability conditions. Using this method, we generated an inclusive data set for the second step; training of the forward model, "FWD net". The forward model exhibits decent generalizability, which was validated in terms of material dispersion, source polarization, and wavelength range of operation. At the final step, we realized inverse optimization under the fabrication constraints. The latent space of the FWD net was taken as our design space to enable design of free-form yet manufacturable meta-atoms. The FWD net is also used as surrogate model in the inverse optimization. The efficacy of our framework was demonstrated by several metadevice examples; a forward-designed metalens, two inverse-designed polarization filters, and an inverse-designed quarter-wave plate. These devices attain the primary functionalities as well as meet the fabrication feasibility. We point out two promising directions for future work including, but not limited to, (i) extension to general meta-atom topologies, and (ii) construction of generative models under global/local fabrication constraints.

METHODS

The data set is a set of unit cells that consist of an arbitrary free-form meta-atom sitting on top of a low-index substrate. The refractive index of the substrate is kept constant as 1.45 ($\approx n_{SiO2}$), and the substrate thickness is taken to be infinite. The meta-atoms have free-form cross sections and constant height values that vary between 1.5 to 2.5 μm. They are made of nondispersive and lossless dielectrics with refractive index values between 2 and 4. The side length of the square unit cells are changing between 2 and 2.5 μm. The operating spectral range is defined from 3 to 5 μm and resolved with 101 equally spaced wavelength points. The resulting data set is labeled with corresponding complex valued transmission coefficients, which are obtained from full wave simulations that are based on the finite difference time domain method. The simulations are performed by the commercial package, Lumerical FDTD solutions. Periodic boundary conditions are applied along the x and y directions, while perfectly matching layers (PML) are used on the z boundaries. x-Polarized plane wave source with injection toward the $+z$ direction is located into the substrate. Magnitude and phase of the transmitted light, which is later converted to complex valued transmission coefficient, are obtained from the near-field power monitor. A total number of 20,000 samples as combination of 400 shapes and 50 parameter sets are generated and labeled by simulations. Twenty percent of the data set is separated as a validation set, and the rest is used for training of both the autoencoder and FC net. Tensorflow is used. We train all the models using an Adam optimizer,[41] mean squared error (MSE) as the loss function. "relu" and "tanh" as activation functions are employed in the autoencoder and FC net, respectively.

To run GA for inverse design, we used the pymoo (multi-objective optimization in Python) library.[42] The library offers parameter-less constraint handling by feasibility-first ranking in a population. Building on the approach, we addressed the constrained inverse optimization problems introduced without case-specific tuning of any constraint parameters.

ASSOCIATED CONTENT

Supporting Information

The Supporting Information is available free of charge at https://pubs.acs.org/doi/10.1021/acsphotonics.2c01006.

Dataset generation; learning curves and error distributions of the models; additional examples from the validation set; forward design of a metalens; explanation of spectral generalizability; additional examples on spectral generalizability; inverse design with varying secondary design variables; comparison of the inverse-designed quarter-wave plate with the forward-designed quarter-wave plates (PDF)

AUTHOR INFORMATION

Corresponding Authors

Wei Chen − *Department of Mechanical Engineering, Northwestern University, Evanston, Illinois 60208, United States;* orcid.org/0000-0002-4653-7124; Email: weichen@northwestern.edu

Koray Aydin − *Department of Electrical and Computer Engineering, Northwestern University, Evanston, Illinois 60208, United States;* orcid.org/0000-0002-3268-2216; Email: aydin@northwestern.edu

Authors

Ibrahim Tanriover − *Department of Electrical and Computer Engineering, Northwestern University, Evanston, Illinois 60208, United States;* orcid.org/0000-0003-1207-7016

Doksoo Lee − *Department of Mechanical Engineering, Northwestern University, Evanston, Illinois 60208, United States;* orcid.org/0000-0002-4597-6643

Complete contact information is available at: https://pubs.acs.org/10.1021/acsphotonics.2c01006

Author Contributions

I.T. and D.L. contributed equally to this work.

Notes

The authors declare no competing financial interest.

https://doi.org/10.1021/acsphotonics.2c01006
ACS Photonics 2023, 10, 875−883

■ ACKNOWLEDGMENTS

Air Force Office of Scientific Research Award FA9550-17-1-0348; National Science Foundation CSSI program Award OAC 1835782; Predictive Science and Engineering Design (PSED) Program at Northwestern University.

■ REFERENCES

(1) Tanriover, I.; Demir, H. V. Broad-Band Polarization-Insensitive All-Dielectric Metalens Enabled by Intentional off-Resonance Waveguiding at Mid-Wave Infrared. *Appl. Phys. Lett.* **2019**, *114* (4), 043105.
(2) Arbabi, A.; Horie, Y.; Ball, A. J.; Bagheri, M.; Faraon, A. Subwavelength-Thick Lenses with High Numerical Apertures and Large Efficiency Based on High-Contrast Transmitarrays. *Nat. Commun.* **2015**, *6* (May), 2−7.
(3) Khorasaninejad, M.; Chen, W. T.; Devlin, R. C.; Oh, J.; Zhu, A. Y.; Capasso, F. Metalenses at Visible Wavelengths: Diffraction-Limited Focusing and Subwavelength Resolution Imaging. *Science.* **2016**, *352* (6290), 1190−1194.
(4) Hadibrata, W.; Wei, H.; Krishnaswamy, S.; Aydin, K. Inverse Design and 3D Printing of a Metalens on an Optical Fiber Tip for Direct Laser Lithography. *Nano Lett.* **2021**, *21* (6), 2422−2428.
(5) Callewaert, F.; Velev, V.; Jiang, S.; Sahakian, A. V.; Kumar, P.; Aydin, K. Inverse-Designed Stretchable Metalens with Tunable Focal Distance. *Appl. Phys. Lett.* **2018**, *112* (9), 091102.
(6) Roberts, J. A.; Yu, S.-J.; Ho, P.-H.; Schoeche, S.; Falk, A. L.; Fan, J. A. Tunable Hyperbolic Metamaterials Based on Self-Assembled Carbon Nanotubes. *Nano Lett.* **2019**, *19* (5), 3131−3137.
(7) Zhan, A.; Colburn, S.; Dodson, C. M.; Majumdar, A. Metasurface Freeform Nanophotonics. *Sci. Rep.* **2017**, *7* (1), 1673.
(8) Pestourie, R.; Pérez-Arancibia, C.; Lin, Z.; Shin, W.; Capasso, F.; Johnson, S. G. Inverse Design of Large-Area Metasurfaces. *Opt. Express* **2018**, *26* (26), 33732−33747.
(9) Zhang, F.; Pu, M.; Li, X.; Gao, P.; Ma, X.; Luo, J.; Yu, H. All-Dielectric Metasurfaces for Simultaneous Giant Circular Asymmetric Transmission and Wavefront Shaping Based on Asymmetric Photonic Spin − Orbit Interactions. *Adv. Funct. Mater.* **2017**, *1704295* (27), 1704295.
(10) Lalau-Keraly, C. M.; Bhargava, S.; Miller, O. D.; Yablonovitch, E. Adjoint Shape Optimization Applied to Electromagnetic Design. *Opt. Express* **2013**, *21* (18), 21693−21701.
(11) Wang, S.; Zhan, Q. Reflection Type Metasurface Designed for High Efficiency Vectorial Field Generation. *Sci. Rep.* **2016**, *6* (1), 29626.
(12) Tanriover, I.; Hadibrata, W.; Scheuer, J.; Aydin, K. Neural Networks Enabled Forward and Inverse Design of Reconfigurable Metasurfaces. *Opt. Express* **2021**, *29* (17), 27219−27227.
(13) Lin, H.; Hou, J.; jin, J.; Wang, Y.; Tang, R.; Shi, X.; Tian, Y.; Xu, W. Machine-Learning-Assisted Inverse Design of Scattering Enhanced Metasurface. *Opt. Express* **2022**, *30* (2), 3076−3088.
(14) Gao, F.; Zhang, Z.; Xu, Y.; Zhang, L.; Yan, R.; Chen, X. Deep-Learning-Assisted Designing Chiral Terahertz Metamaterials with Asymmetric Transmission Properties. *J. Opt. Soc. Am. B* **2022**, *39* (6), 1511−1519.
(15) Seo, D.; Nam, D. W.; Park, J.; Park, C. Y.; Jang, M. S. Structural Optimization of a One-Dimensional Freeform Metagrating Deflector via Deep Reinforcement Learning. *ACS Photonics* **2022**, *9* (2), 452−458.
(16) Yeung, C.; Tsai, J.-M.; King, B.; Pham, B.; Ho, D.; Liang, J.; Knight, M. W.; Raman, A. P. Multiplexed Supercell Metasurface Design and Optimization with Tandem Residual Networks. *Nanophotonics* **2021**, *10* (3), 1133−1143.
(17) Tanriover, I.; Hadibrata, W.; Aydin, K. Physics-Based Approach for a Neural Networks Enabled Design of All-Dielectric Metasurfaces. *ACS Photonics* **2020**, *7* (8), 1957−1964.
(18) An, S.; Fowler, C.; Zheng, B.; Shalaginov, M. Y.; Tang, H.; Li, H.; Zhou, L.; Ding, J.; Agarwal, A. M.; Rivero-Baleine, C.; Richardson, K. A.; Gu, T.; Hu, J.; Zhang, H. A Deep Learning Approach for Objective-Driven All-Dielectric Metasurface Design. *ACS Photonics* **2019**, *6* (12), 3196−3207.
(19) Luo, J.; Li, X.; Zhang, X.; Guo, J.; Liu, W.; Lai, Y.; Zhan, Y.; Huang, M. Deep-Learning-Enabled Inverse Engineering of Multi-Wavelength Invisibility-to-Superscattering Switching with Phase-Change Materials. *Opt. Express* **2021**, *29* (7), 10527.
(20) Zhelyeznyakov, M. V.; Brunton, S.; Majumdar, A. Deep Learning to Accelerate Scatterer-to-Field Mapping for Inverse Design of Dielectric Metasurfaces. *ACS Photonics* **2021**, *8* (2), 481−488.
(21) Nadell, C. C.; Huang, B.; Malof, J. M.; Padilla, W. J. Deep Learning for Accelerated All-Dielectric Metasurface Design. *Opt. Express* **2019**, *27* (20), 27523.
(22) Liu, Z.; Zhu, D.; Rodrigues, S. P.; Lee, K. T.; Cai, W. Generative Model for the Inverse Design of Metasurfaces. *Nano Lett.* **2018**, *18* (10), 6570−6576.
(23) An, S.; Zheng, B.; Shalaginov, M. Y.; Tang, H.; Li, H.; Zhou, L.; Ding, J.; Agarwal, A. M.; Rivero-Baleine, C.; Kang, M.; Richardson, K. A.; Gu, T.; Hu, J.; Fowler, C.; Zhang, H. Deep Learning Modeling Approach for Metasurfaces with High Degrees of Freedom. *Opt. Express* **2020**, *28* (21), 31932.
(24) Inampudi, S.; Mosallaei, H. Neural Network Based Design of Metagratings. *Appl. Phys. Lett.* **2018**, *112* (24), 241102.
(25) Ma, W.; Cheng, F.; Xu, Y.; Wen, Q.; Liu, Y. Probabilistic Representation and Inverse Design of Metamaterials Based on a Deep Generative Model with Semi-Supervised Learning Strategy. *Adv. Mater.* **2019**, *31* (35), 1901111.
(26) Wang, L.; Chan, Y. C.; Ahmed, F.; Liu, Z.; Zhu, P.; Chen, W. Deep Generative Modeling for Mechanistic-Based Learning and Design of Metamaterial Systems. *Comput. Methods Appl. Mech. Eng.* **2020**, *372*, 113377.
(27) Nie, Z.; Lin, T.; Jiang, H.; Kara, L. B. TopologyGAN: Topology Optimization Using Generative Adversarial Networks Based on Physical Fields over the Initial Domain. *Proc. ASME Des. Eng. Technol. Conf.* 2020, *11A-2020*, DOI: 10.1115/DETC2020-22675.
(28) Chen, M.; Jiang, J.; Fan, J. A. Design Space Reparameterization Enforces Hard Geometric Constraints in Inverse-Designed Nanophotonic Devices. *ACS Photonics* **2020**, *7* (11), 3141−3151.
(29) Qu, Y.; Jing, L.; Shen, Y.; Qiu, M.; Soljačić, M. Migrating Knowledge between Physical Scenarios Based on Artificial Neural Networks. *ACS Photonics* **2019**, *6* (5), 1168−1174.
(30) Peurifoy, J.; Shen, Y.; Jing, L.; Yang, Y.; Cano-Renteria, F.; DeLacy, B. G.; Joannopoulos, J. D.; Tegmark, M.; Soljačić, M. Nanophotonic Particle Simulation and Inverse Design Using Artificial Neural Networks. *Sci. Adv.* **2018**, *4* (6), 1.
(31) Sajedian, I.; Kim, J.; Rho, J. Finding the Optical Properties of Plasmonic Structures by Image Processing Using a Combination of Convolutional Neural Networks and Recurrent Neural Networks. *Microsystems Nanoeng.* **2019**, *5* (1), 27.
(32) Inampudi, S.; Mosallaei, H. Neural Network Based Design of Metagratings. *Appl. Phys. Lett.* **2018**, *112* (24), 241102.
(33) Liu, D.; Tan, Y.; Khoram, E.; Yu, Z. Training Deep Neural Networks for the Inverse Design of Nanophotonic Structures. *ACS Photonics* **2018**, *5* (4), 1365−1369.
(34) Seo, D.; Nam, D. W.; Park, J.; Park, C. Y.; Jang, M. S. Structural Optimization of a One-Dimensional Freeform Metagrating Deflector via Deep Reinforcement Learning. *ACS Photonics* **2022**, *9* (2), 452−458.
(35) So, S.; Badloe, T.; Noh, J.; Rho, J.; Bravo-Abad, J. Deep Learning Enabled Inverse Design in Nanophotonics. *Nanophotonics* **2020**, *9* (5), 1041−1057.
(36) Piggott, A. Y.; Petykiewicz, J.; Su, L.; Vučković, J. Fabrication-Constrained Nanophotonic Inverse Design. *Sci. Rep.* **2017**, *7* (1), 1786.
(37) McKay, M. D.; Beckman, R. J.; Conover, W. J. A Comparison of Three Methods for Selecting Values of Input Variables in the Analysis of Output from a Computer Code. *Technometrics* **2000**, *42* (1), 55−61.

(38) Kulesza, A.; Taskar, B. Determinantal Point Processes for Machine Learning. *Found. Trends Mach. Learn.* **2012**, *5* (2−3), 123−286.
(39) Mansouree, M.; McClung, A.; Samudrala, S.; Arbabi, A. Large-Scale Parametrized Metasurface Design Using Adjoint Optimization. *ACS Photonics* **2021**, *8* (2), 455−463.
(40) Colburn, S.; Majumdar, A. Inverse Design and Flexible Parameterization of Meta-Optics Using Algorithmic Differentiation. *Commun. Phys.* **2021**, *4* (1), 65.
(41) Kingma, D. P.; Ba, J. L. Adam: A Method for Stochastic Optimization. 2017-01-30. arXiv (Computer Science, Machine Learning), arXiv:1412.6980 (accessed 2020-01-12).
(42) Blank, J.; Deb, K. Pymoo: Multi-Objective Optimization in Python. *IEEE Access* **2020**, *8*, 89497−89509.

https://doi.org/10.1021/acsphotonics.2c01006
ACS Photonics 2023, 10, 875−883